Numerical Investigation on Silt Particle Abrasion Characteristics of the Centrifugal Pump

Xiangdong Han[1], Youchao Yang[2], Chao Wang[2,4], Pengjun Fan[3], and Yaping Tian[5(✉)]

[1] School of Civil Engineering, Nanchang Institute of Technology, Nanchang 330044, China
[2] Chongqing Pump Industry Co., Ltd., Chongqing 400033, China
[3] Machine Industry Lanzhou Petrochemical Equipment Inspection Institute Co., Ltd., Lanzhou 730070, China
[4] College of Aerospace and Civil Engineering, Harbin Engineering University, Harbin 150001, China
[5] Gansu Water Resources and Hydroelectric Investigation and Design and Research Institute Corporation Limited, Lanzhou 730000, China
typ_pj@163.com

Abstract. Silt particle abrasion characteristics of the centrifugal pump were numerically investigated. Mean diameter of the employed silt particles was 0.025 mm and the concentration was 1%. Results indicated that for diverse pressure and suction surfaces, distributions of silt particle mass concentration were various. The distribution scope on suction surface was larger than that of the pressure surface. Silt particle abrasion rate on suction surface was greater than in the pressure surface. They were alternation change. The laws on suction surface were contrary to that of pressure surface. The investigations could provide theoretical supports for engineering applications in hydraulic machinery engineering fields.

Keywords: Silt particle mass concentration · Silt particle abrasion rate · Centrifugal pump · Numerical simulation

1 Introduction

Centrifugal pump is one kind of typical hydraulic machinery [1]. When it operates in rivers containing silt particles and suspended sediments, the components could be destroyed by silt particle abrasion severely [2], such as centrifugal pumps in *Jingdian* irrigation area of Gansu province. It is the solid-liquid two-phase flow [3]. Silt particle abrasion has close relation with the properties of silt particles [4], such as concentration, diameter, and impact angle (Fig. 1).

Many scholars have performed corresponding investigations. Serrano et al. [5] assessed the role of particle concentration on destructions of the centrifugal pump impeller; they acquired that the abrasion could be reduced significantly via the control on impeller rotational speed according to the concentration and water level. Li et al. [6] experimentally and numerically studied the abrasion characteristics in one

L. Yan and J. Na (Eds.): ICFPMCE 2022, AHE 10, pp. 241–250, 2023.
https://doi.org/10.2991/978-94-6463-022-0_21

Fig. 1. Destroyed impeller of the centrifugal pump in *Jingdian* irrigation area.

solid-liquid centrifugal pump; they got that under various silt particle concentrations, abrasion degrees were diverse. Wang and Qian [7] achieved investigations of effects of particle concentration and mean diameter on variations of head and efficiency of one certain double-suction centrifugal pump. Khalid and Sapuan [8] discussed effects of silt particles on losses of weight, diameter, blade thickness, and blade height of one centrifugal slurry pump impeller and thickness change of this impeller. Zhang et al. [9] performed numerical analysis of silt particle-water two-phase flow characteristics in one centrifugal pump during the startup period.

Investigations on silt particle-water two-phase flow in the centrifugal pump were relatively abundant. However, detailed discussions of related particle distribution characteristics on pressure surface (PS) and suction surface (SS) of every blade of the impeller were particularly few. Therefore, we performed this study. The mean diameter was 0.025 mm and the concentration was 1%.

2 Mathematical Model

2.1 Fundamental Equations

For numerical simulation of silt particle-water two-phase flow, water was the primary phase, which was the continuous medium. Continuity equation and momentum equation [10] were employed to show the flow characteristics of water in the centrifugal pump.

$$\frac{\partial}{\partial x_i}(\rho_l u_i) = 0 \tag{1}$$

$$\frac{\partial}{\partial x_i}(\rho_l u_i) + \frac{\partial}{\partial x_j}\left(\rho_l u_i u_j\right) = -\frac{\partial p}{\partial x_i} + \frac{\partial}{\partial x_j}\left[\mu\left(\frac{\partial u_i}{\partial x_j} + \frac{\partial u_j}{\partial x_i}\right)\right] + \frac{\partial}{\partial x_j}\left(-\overline{\rho_l u_i' u_j'}\right) \tag{2}$$

where ρ_l is water density. u is water velocity and u' is fluctuating velocity. p is pressure. x is coordinate. i and j are subscripts, which indicates directions in the Cartesian coordinate system, taken as 1, 2, and 3, respectively. μ is dynamic viscosity of water.

Silt particles were dispersed medium. Discrete Phase Model (DPM) in commercial software ANSYS-Fluent [11] was employed to describe their flow characteristics, which primarily solved the balance of different forces acting on silt particles. The equations are as following:

$$\frac{du_{\mathrm{p}}}{dt} = F_{\mathrm{D}}\left(\overrightarrow{u} - \overrightarrow{u_{\mathrm{p}}}\right) + \frac{\overrightarrow{g}\left(\rho_{\mathrm{p}} - \rho_{\mathrm{l}}\right)}{\rho_{\mathrm{p}}} \tag{3}$$

where u_{p} is velocity of silt particles, t is time, g is gravitational acceleration, and ρ_{p} is density of silt particles. F_{D} is the drag, defined as in Eq. (4):

$$F_{\mathrm{D}} = \frac{3}{4}\frac{\mu C_D \mathrm{Re}_{\mathrm{p}}}{\rho_{\mathrm{p}} d_{\mathrm{p}}^2} \tag{4}$$

where Re_{p} is Reynolds number of silt particles and d_{p} is silt particle mean diameter. C_{D} is drag coefficient.

2.2 Turbulence Model

Shear Stress Transport (SST) k-ω turbulence model [12] was employed to show turbulent flow characteristics in the centrifugal pump. It combined the advantages of k-ω and k-ε turbulence models. The significant merit was that this model was particularly robust.

$$\rho_{\mathrm{l}}\frac{\partial k}{\partial t} + \rho_{\mathrm{l}}\overline{u_j}\frac{\partial k}{\partial x_j} = P_k - \rho_{\mathrm{l}}\beta_* \omega k + \frac{\partial}{\partial x_j}\left[\left(\mu + \frac{\mu_{\mathrm{t}}}{\sigma_k}\right)\frac{\partial k}{\partial x_j}\right] \tag{5}$$

$$\rho_{\mathrm{l}}\frac{\partial \omega}{\partial t} + \rho_{\mathrm{l}}\overline{u_j}\frac{\partial \omega}{\partial x_j} = \alpha P_\omega - \rho_{\mathrm{l}}\beta_* \omega^2 + \frac{\partial}{\partial x_j}\left[\left(\mu + \frac{\mu_{\mathrm{t}}}{\sigma_\omega}\right)\frac{\partial \omega}{\partial x_j}\right] + 2\rho_{\mathrm{l}}(1 - F_B)\frac{1}{\sigma_{\omega_{\mathrm{out}}}\omega}\frac{\partial k}{\partial x_j}\frac{\partial \omega}{\partial x_j} \tag{6}$$

where k is turbulent kinetic energy and P_k is the corresponding production term. ω is specific dissipation rate and P_ω is the corresponding production term. μ_{t} is eddy viscosity. F_{B} is one blending function. α, σ_k, and σ_ω are empirical coefficients. β_* and $\sigma_{k\mathrm{out}}$ are taken as 0.09 and 1.168, respectively.

2.3 Silt Particle Abrasion Rate Prediction Model

Silt particle abrasion rate prediction model built into ANSYS-Fluent [13] was employed to assess abrasion rate in the centrifugal pump. The model was widely used in numerical simulation to analyze the destruction characteristics caused by silt particles.

$$R_{\mathrm{abrasion}} = \sum_{p=1}^{N_{\mathrm{silt\ particles}}} \frac{m_{\mathrm{s}} C(d_1) f(\alpha) v^{b(v)}}{A_{\mathrm{face}}} \tag{7}$$

where R_{abrasion} is silt particle abrasion rate. $N_{\mathrm{silt\ particles}}$ is total number of silt particles. m_{s} is silt particle mass. $C(d_1)$ is one function of silt mean diameter. α is impact angle between silt particle path with wall face; $f(\alpha)$ is the corresponding function. v is silt particle relative velocity; $b(v)$ is the corresponding function. A_{face} is cell face area at the wall.

3 Numerical Simulation Setup

3.1 Physical Model

Centrifugal pump with the type: M196-100 was employed to perform the investigations of silt particle-water two-phase flow.

It mainly included four different components: suction pipe, impeller, volute, and exit pipe, as shown in Fig. 2.

Primary performance parameters were that designed flow rate $Q_d = 100$ m^3/h, designed head $H_d = 21$ m, and rotational speed $n_r = 2900$ rpm.

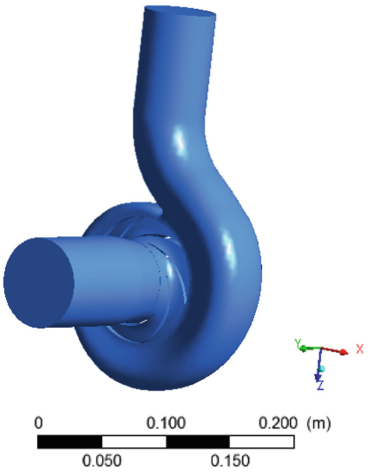

Fig. 2. Physical model of the centrifugal pump.

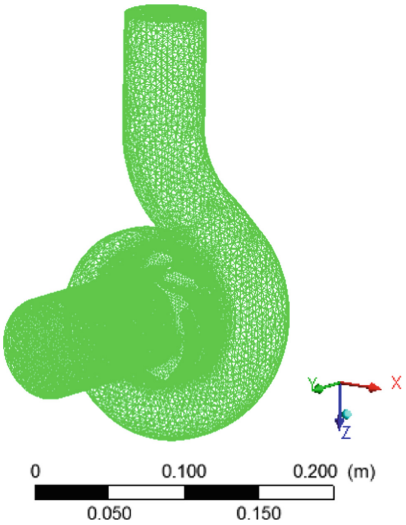

Fig. 3. Unstructured meshes of the centrifugal pump.

Impeller was the core component of the centrifugal pump, which converted energy of the prime mover into the water. Main geometrical parameters of the impeller were that impeller inlet diameter was $D_j = 89$ mm, impeller outlet diameter was $D_2 = 140$ mm, impeller outlet width was $b_2 = 27$ mm, blade wrap angle $\varphi = 105°$, and blade number $Z = 6$.

3.2 Mesh Generation

ANSYS-ICEM was utilized to discretize the centrifugal pump computational domain. Comprehensively considering complex structures of the impeller and volute, unstructured meshes were generated to perform the discretization of all computational domains. Mesh size and node density could be controlled easily. Moreover, mesh adaption were achieved conveniently. Total mesh number was 1802098. The quality was higher than 0.27 (Fig. 3).

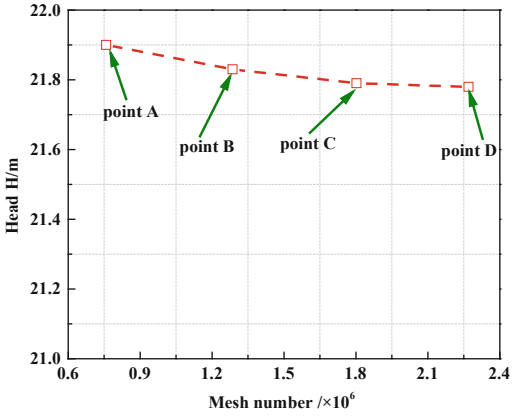

(a) Head

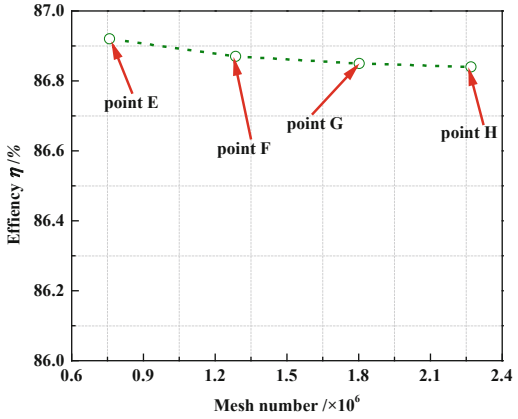

(b) Efficiency

Fig. 4. Mesh independence check and numerical uncertainty analysis.

Head and efficiency under diverse total mesh numbers were calculated to perform mesh independence check and numerical uncertainty analysis. With the increase of mesh number (from point A to point B for the head and from point E to point F for the efficiency), they decreased a little more significantly. Then, the respective difference was particularly small (from point B to point D for the head and from point F to point H for the efficiency). For the head, the maximum difference was less than 0.23%. For the efficiency, it was less than 0.026% (Fig. 4).

4 Results and Discussion

For all pressure surfaces, the most remarkable feature was that distribution regions of silt particle mass concentration were particularly minute; it indicated that effects of silt particles were relatively weak. Detailed analysis was that at PS-1, the primary regions were at the bottom-right. They were scattered, the most significant peculiarity. For PS-2, main regions were at the middle and bottom of the right parts and the shape was strip. At PS-3, a few minute regions existed at the bottom-left and middle parts; distributions were dispersed, similar with those of PS-1. However, the scope was smaller than in PS-1. For PS-4, upper-left and bottom-right parts were destroyed by silt particles. However, the distribution regions were especially minute. At PS-5, the shape was strip as well, identical with that of PS-2. While the locations were different from those of PS-2. They were at the middle and peak of the left parts. For PS-6, primary regions were at the bottom of the surface. Some particularly minute regions were at the upper parts. The general law was that total distribution regions on different pressure surfaces were particularly small, which indicated that effects of silt particles with $\alpha_s = 1\%$ on destructions of diverse pressure surfaces were relatively weak (Fig. 5).

Moreover, distribution regions on different suction surfaces were various as well. At SS-1, regions damaged were mainly at middle and bottom parts of the right side. Also, a few regions existed at bottom parts of the left side. For SS-2, regions were smaller than in SS-1. Main parts were at the bottom of the left side, different from that of SS-1. Some particularly small regions were at upper parts of the left side and middle parts of the right side. At SS-3, primary regions were at the bottom of the surface. Some dispersive regions were at upper and middle parts. The regions were larger than those of SS-2. For SS-4, the destroyed ones mainly distributed at the middle and bottom parts of the surface. Some were at the left side; the distributions were scattered. Some were at the right side and the shape was strip; At SS-5, the primary distribution regions were contrary to each other. Some regions were located at the bottom-left parts; while some were at the upper-right. For SS-6, regions which were damaged by silt particle abrasion were at the bottom-left parts and a few scattered regions were at the bottom-right parts (Fig. 6).

Variations of silt particle abrasion rate accurately reflected distribution characteristics of silt particle mass concentration on different surfaces. The rates of suction surfaces were greater than in pressure surfaces, which was consistent with that the distribution areas of suction surfaces were larger than those of pressure surfaces and the destruction intensity was stronger than in pressure surfaces as well. Variations of the rate on pressure and suction surfaces were alternate change. However, the overall laws of variation were contrary to each other (Fig. 7).

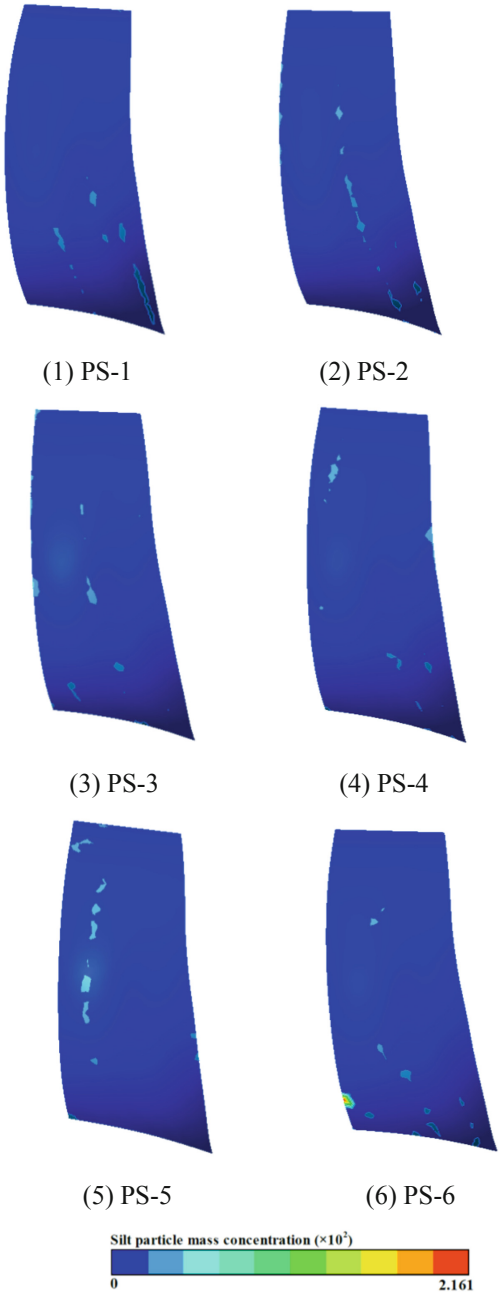

Fig. 5. Distribution characteristics of silt particle mass concentration at different pressure surfaces.

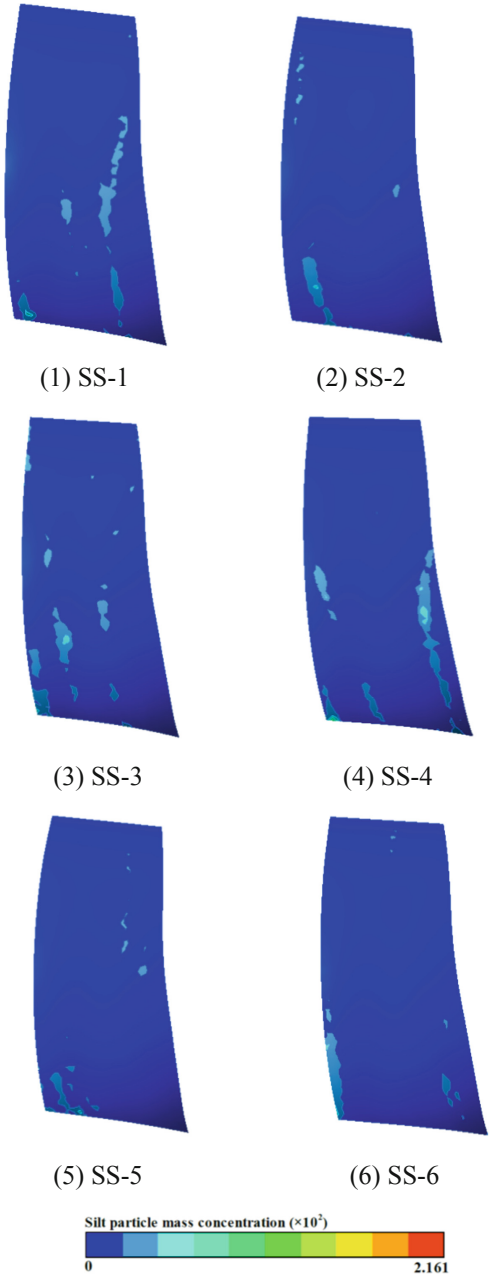

Fig. 6. Distribution characteristics of silt particle mass concentration at different suction surfaces.

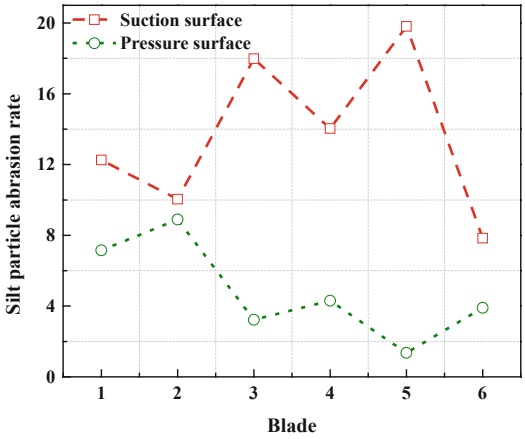

Fig. 7. Variations of silt particle abrasion rate on different pressure and suction surfaces.

5 Conclusions

Silt particle-water two-phase flow in the centrifugal pump was numerically simulated. Silt particle mean diameter was 0.025 mm and the concentration was 1.0%. Distributions of silt particle mass concentration on all pressure and suction surfaces and variations of corresponding abrasion rate were discussed. Main conclusions were as follows:

(1) Distributions of silt particle mass concentration on different pressure and suction surfaces were various.
(2) All distribution regions on different suction surfaces were larger than those on pressure surfaces.
(3) Silt particle abrasion rate on pressure surface was greater than that of suction surface. Variations were alternate. The laws for suction surface were contrary to those of pressure surface.

Acknowledgments. The investigation was financially supported by National Natural Science Foundation of China (Grant No. 52169018).

References

1. Tuzson, J.: Centrifugal Pump Design. Wiley (2000)
2. Duan, C.G., Karelin, V.Y.: Abrasive Erosion and Corrosion of Hydraulic Machinery. Imperial College Press (2002)
3. Peker, S.M., Helvaci, S.S.: Solid-Liquid Two Phase Flow. Elsevier (2008)
4. Kleis, I.,Kulu, P.: Solid Particle Erosion Occurrence, Prediction and Control. Springer, Cham (2007). https://doi.org/10.1007/978-1-84800-029-2
5. Serrano, R.O.P., Santos, L.P., Viana, E.M.F., Pinto, M.A., Martinez, C.B.: Case study: effects of sediment concentration on the wear of fluvial water pump impellers on Brazil's Acre River. Wear **408–409**, 131–137 (2018). https://doi.org/10.1016/j.wear.2018.04.018

6. Li, Y., Zhu, Z.C., He, Z.H., He, W.Q.: Abrasion characteristic analyses of solid-liquid two-phase centrifugal pump. J. Therm. Sci. **20**(3), 283–287 (2011). https://doi.org/10.1007/s11630-011-0471-8
7. Wang, Z.Y., Qian, Z.D.: Effects of concentration and size of silt particles on the performance of a double-suction centrifugal pump. Energy **123**, 36–46 (2017). https://doi.org/10.1016/j.energy.2017.01.142
8. Khalid, Y.A., Sapuan, S.M.: Wear analysis of centrifugal slurry pump impellers. Ind. Lubr. Tribol. **59**(1), 18–28 (2007). https://doi.org/10.1108/00368790710723106
9. Zhang, Y.L., Li, Y., Zhu, Z.C., Cui, B.L.: Computational analysis of centrifugal pump delivering solid-liquid two-phase flow during startup period. Chin. J. Mech. Eng. **27**(1), 178–184 (2014). https://doi.org/10.3901/CJME.2014.01.178
10. Mueller, J.D.: Essentials of Computational Fluid Dynamics. CRC Press (2020)
11. Zahari, N.M., et al.: Introduction of discrete phase model (DPM) in fluid flow: a review. In: Proceedings of the 4th International Conference on Green Design and Manufacture, 020234 (2018)
12. Wilcox, D.C.: Simulation of transition with a two-equation turbulence model. AIAA J. **32**(2), 247–255 (1994). https://doi.org/10.2514/3.59994
13. ANSYS. Inc.: ANSYS Fluent Theory Guide (2020)